ORNL/CP-101232

SURFACE ENGINEERING OF SILICON AND CARBON BY PULSED-LASER ABLATION

Douglas H. Lowndes [*], Vladimir I. Merkulov [*],
Antonio J. Pedraza [**], Jason D. Fowlkes [**],
A. A. Puretzky [*], D. B. Geohegan [*], and G. E. Jellison, Jr. [*]

[*] Solid State Division, Oak Ridge National Laboratory,
P. O. Box 2008, Oak Ridge, TN 37831-6056

[**] Dept. of Materials Science and Engineering, The University of Tennessee,
Knoxville, TN 37996-2200

Invited Paper Submitted for the

TMS Annual Meeting
Symposium on Surface Engineering: Science and Technology I

San Diego, CA
February 28–March 4, 1999

November 1998

Prepared by
Solid State Division
Oak Ridge National Laboratory
P.O. Box 2008
Oak Ridge, Tennessee 37831-6056
managed by
LOCKHEED MARTIN ENERGY RESEARCH CORP.
for the
U.S. DEPARTMENT OF ENERGY
under contract DE-AC05-96OR22464

DISCLAIMER

DISCLAIMER

Portions of this document may be illegible in electronic image products. Images are produced from the best available original document.

SURFACE ENGINEERING OF SILICON AND CARBON BY PULSED LASER ABLATION

Douglas H. Lowndes,[a, b] Vladimir I. Merkulov,[a]
Antonio J. Pedraza,[b] Jason D. Fowlkes,[b]
A. A. Puretzky,[a] D. B. Geohegan,[a] and G. E. Jellison, Jr.[a]

[a] Solid State Division, Oak Ridge National Laboratory, Oak Ridge, TN 37831-6056
[b] Department of Materials Science and Engineering, The University of Tennessee, Knoxville, TN 37996-2200

Abstract

Experiments are described in which a focused pulsed-excimer laser beam is used either to ablate a graphite target and deposit hydrogen-free amorphous carbon films, or to directly texture a silicon surface and produce arrays of high-aspect-ratio silicon microcolumns.

In the first case, diamond-like carbon (or tetrahedral amorphous carbon, ta-C) films were deposited with the experimental conditions selected so that the masses and kinetic energies of incident carbon species were reasonably well controlled. Striking systematic changes in ta-C film properties were found. The sp^3-bonded carbon fraction, the valence electron density, and the optical (Tauc) energy gap all reach their maximum values in films deposited at a carbon ion kinetic energy of ~90 eV. Tapping-mode atomic force microscope measurements also reveal that films deposited at 90 eV are extremely smooth (rms roughness ~1 Å over several hundred nm) and relatively free of particulates, while the surface roughness increases in films deposited at significantly lower energies.

In the second set of experiments, dense arrays of high-aspect-ratio silicon microcolumns ~20–40 μm tall and ~2 μm in diameter were formed by cumulative nanosecond pulsed excimer laser irradiation of silicon wafers in air and other oxygen-containing atmospheres. It is proposed that microcolumn growth occurs through a combination of pulsed-laser melting of the tips of the columns and preferential redeposition of silicon on the molten tips from the ablated flux of silicon-rich vapor.

The common theme in this research is that a focused pulsed-laser beam can be used quite generally to create an energetic flux, either the energetic carbon ions needed to form sp^3 (diamond-like) bonds or the overpressure of silicon-rich species needed for microcolumn growth. Thus, new materials synthesis opportunities result from the access to nonequilibrium growth conditions provided by pulsed-laser ablation.

1. Deposition of Hydrogen-Free Amorphous Carbon Films

Background

Deposition of hard carbon-film coatings using energetic-beam sources was first reported more than two decades ago [1, 2]. More recent studies have focused on the structure and properties of hydrogen-free amorphous diamond films (also known as tetrahedral amorphous carbon, ta-C) that contain a large fraction (75-85%) of sp^3-bonded (tetrahedrally-coordinated) carbon atoms. [3-5] These ta-C films have distinctly different properties than the hydrogen-containing amorphous carbon films (denoted by a-C:H) that have been deposited by CVD methods. ta-C films have been synthesized using a variety of energetic-beam methods [6] including filtered cathodic vacuum arc (FCVA) [7–14], mass-separated ion beam deposition (MSIBD) [15–17], and pulsed laser ablation (PLA) [18–40]. The useful properties of ta-C films with high sp^3 content include high hardness and Young's modulus, scratch-resistance, chemical inertness, a low coefficient of friction, high transparency in the visible region associated with a moderately wide (≥2 eV) optical (Tauc) band gap, and good thermal conductivity [3–5].

Recent pulsed-laser deposition experiments in our laboratory [34–36] as well as recent studies using the FCVA method [10–14] show that the sp^3-bonded fraction, optical (Tauc) band gap, index of refraction, and electrical resistivity all reach their maximum values for incident carbon ion kinetic energies of 80–100 eV, i.e. this appears to be the optimum energy range to produce highly diamond-like ta-C films by PLA and FCVA. [34, 35, 41, 42] This result was not obtained from earlier PLA experiments because with PLA it is usually difficult to control the kinetic energy, KE, of depositing species since the ablated flux normally consists of a variety of neutral and ionized carbon atoms, dimers and trimers with different masses and KE. Earlier experiments using FCVA and other methods also showed that films with nearly maximal sp^3 content as well as highly diamond-like properties could be produced using carbon ions whose KE ranged from ~20 eV to at least several hundred eV [7–9, 15–17].

However, in our recent studies of PLA ta-C films an ArF pulsed excimer laser operating at 193 nm wavelength was used to produce the carbon-ion flux, with two significant advantages. First, earlier measurements by Puretzky and Geohegan showed that for ArF-laser ablation of a graphite target the ablated flux consists primarily of *monatomic* neutral and ionized species (C, C^+, C^{2+}) even at relatively low fluences [23, 24]. Consequently, the dominant mass of ablated species is known so that time-of-flight measurements, using an in situ ion probe, provide a simple, accurate method of determining the KE and its dispersion. Such ion probe measurements also are readily transferable for inter-laboratory comparisons. Second, we found that much higher C^+ ion KE values are produced by ArF-laser ablation than by KrF (or longer wavelength) ablation for any given laser fluence and spot size. This somewhat reduces the need for very high fluences and tight beam-focusing on the target that are encountered at longer laser wavelengths. We note that Koster and Mann recently reported that an even more dramatic increase of C^+ KE can be obtained by reducing the laser pulse duration from the nanosecond to the sub-picosecond regime at fixed wavelength. [29]

Because of the difficulty of directly measuring the KE of the depositing species, there is still little information available regarding how the surface morphology and properties of PLA amorphous carbon (a-C) films evolve as a function of deposition energy. [43] Consequently, in this paper we report additional results from our systematic study [34–36] of changes in the surface morphology and roughness, bonding, and optical properties of hydrogen-free PLA a-C films as a function of the KE measured using an in situ ion probe, with particular emphasis here on KE values far from the ~90 eV optimum value that produces the most diamond-like properties (i.e. ta-C).

Experimental

Film Deposition. The two deposition systems and the procedures used in this work have been described elsewhere. [34, 35]. Briefly, films were deposited in two vacuum chambers evacuated by turbomolecular pumps to a base pressure of 3×10^{-8} torr. The pulsed ArF laser beam was incident at 45° onto 2.54-cm diameter pyrolytic graphite targets containing < 10 ppm total

impurities (Specialty Minerals, Inc., Easton, PA). A lens was positioned at its focal distance from the target, which rotated continuously (20 rpm) during ablation.

Kinetic Energy Measurements. An ion probe [44] was used to measure the travel time of ablated ions. The time corresponding to the ion current peak ("icp") was used to calculate a velocity and corresponding kinetic energy, KE_{icp} , for those ions arriving at the peak of the ion current. [34, 35]

Substrates and Film Characterization. The surface structure, bonding, and optical properties of ta-C films were studied using scanning transmission electron microscopy (STEM), electron energy loss spectroscopy (EELS), spectroscopic ellipsometry (SE), and tapping-mode atomic force microscopy (TM-AFM) measurements. For SE measurements, [45] ~70-180 nm-thick ta-C films were deposited on p-type (0.2-0.4 Ω-cm) and n-type (0.008-0.02 Ω-cm) (001)-oriented Si wafers. The substrates were unheated and were mounted on a metal holder located at D_{ts} = 4.8–7.3 cm from the target. Typical ArF-laser deposition rates from ~ 90 eV C^+ ions were ~0.03 Å/shot at D_{ts} = 7.3 cm and ~ 0.1 Å/shot at D_{ts} = 4.8 cm. For EELS measurements, ta-C films ~ 30 nm thick were deposited on freshly cleaved NaCl substrates. The substrates were later dissolved in DI water and the films placed in folding nickel TEM grids. [35] TM-AFM was used rather than contact-mode AFM because other investigators have found that the SiN tips used for contact-mode measurements are quickly damaged by the extreme hardness of ta-C films, resulting in degraded image quality [37].

Interpretation of EELS Measurements. The EELS spectrum in the energy range of the carbon K absorption edge contains several distinctive features. The peak at ~ 285.5 eV is due to electronic transitions from the C 1s ground state to empty p* antibonding states. Transitions from 1s to the higher energy s* states occur at energies ≥ 290 eV. The sp^3 bonding fraction for ta-C films was determined using the standard method of Berger et al. [46]. In this method it is assumed that I_p and I_s, the integrated intensities of the two peaks corresponding to the 1s-p* and 1s-s* electronic transitions, are directly proportional to the number of sp^2- and (sp^2 + sp^3)-bonded C atoms, respectively. The sp^2 fraction, f_{sp^2}, is calculated by taking the ratio of I_p and I_s and normalizing it to the value for a 100% sp^2-bonded carbon sample (see ref. 19). The sp^3 fraction is simply 1 - f_{sp^2}. An arc-evaporated carbon sample was used to obtain a reference EELS spectrum corresponding to entirely sp^2 bonding. EELS spectra also were measured in the low-energy range of valence electron collective excitations (plasmons) near 30 eV in order to correlate changes in the valence electron density (proportional to the plasmon peak energy) with the changing sp^3 fraction, also as a function of the C^+ ion KE_{icp}.

Spectroscopic Ellipsometry. SE measurements were carried out using a new instrument [47] and a new Tauc-Lorentz (TL) model [45] for the dielectric functions of amorphous materials. By fitting the SE data to the TL model it was possible to obtain values for the Tauc (optical) band gap, film thickness, surface roughness, and the film-substrate interface-layer thickness of ta-C films, all as functions of the C^+ ion KE_{icp}. SE measurements of ta-C films deposited on 7.5 cm diam Si substrates also were used to determine the lateral (or angular) variation of film thickness and optical properties and to relate these to independent ion probe measurements of the angular variation of the C^+ KE_{icp} in the ablation plume.

Results and Discussion

sp^3-Bonding Fraction and Plasmon Peak Energy vs Carbon Ion Kinetic Energy. As shown in Fig. 1, EELS measurements in the carbon K-edge energy range (core excitation spectra) revealed that a C^+ ion KE_{icp} ~ 90 eV maximizes the sp^3-bonded carbon fraction in ArF-laser deposited ta-C films. This result is in good agreement with the optimum KE determined recently by several groups for FCVA deposition of ta-C [10-14]. Our ~ 73% maximum sp^3-bonding fraction is slightly lower than maximum values in the mid-80% range reported for FCVA ta-C films, possibly due to the larger spread of KE values for ablation. [34] As shown in Fig. 1, the plasmon energy-loss peak also reached its maximum value (30.9 eV) in ta-C films deposited at KE_{icp} ~ 90 eV. For comparison, the plasmon peak for crystalline diamond is located at ~ 33.8 eV [46]. The plasmon measurements provide an important internal check on the validity of the sp^3 bonding measurements, since in a Drude-like model the energy of the plasmon peak is

proportional to the valence electron density, which is expected to scale with the sp^3 fraction. Consequently, the observed maximization of both the plasmon energy and sp^3 fraction at KE_{icp} ~ 90 eV is consistent with formation of the most diamond-like films at this energy. The remaining reduction in the plasmon peak energy for ta-C, relative to crystalline diamond, corresponds to the decreased ta-C film density that results from both its amorphous state and the presence of some sp^2 bonds [46].

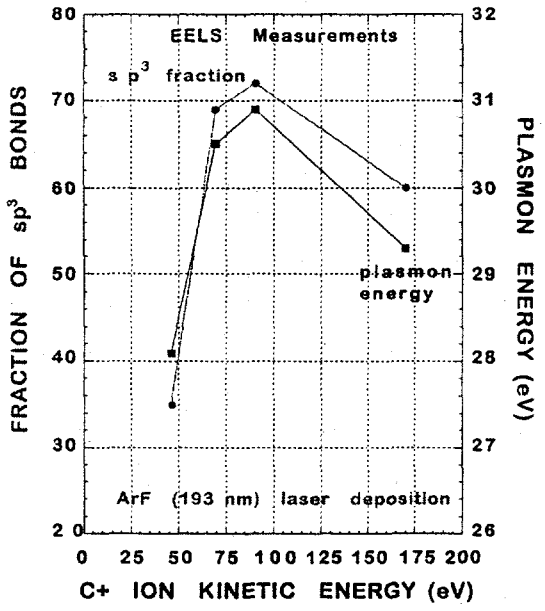

Fig. 1. sp^3 bonding fraction and energy of the plasmon-loss peak of ta-C films vs the C^+ ion KE_{icp} used for film deposition.

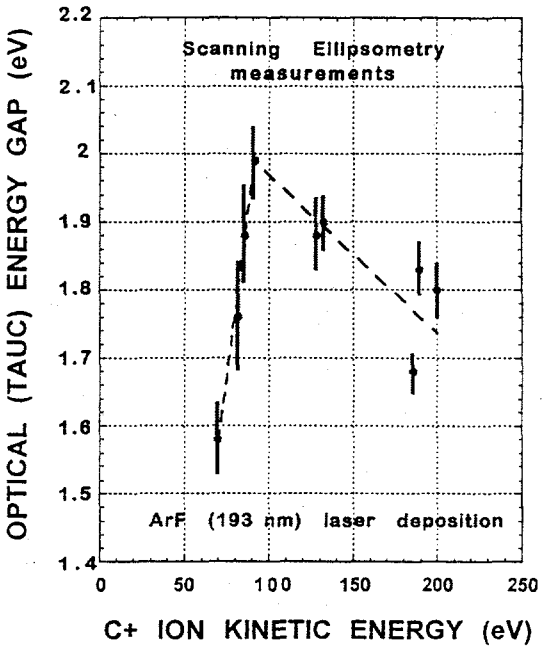

Fig. 2. Optical (Tauc) energy gap of ta-C films vs the C^+ ion KE_{icp} used for film deposition.

Optical Band Gap vs Carbon Ion Kinetic Energy. Spectroscopic ellipsometry (SE) data were fitted using a model of the ta-C dielectric constant in which the optical (Tauc) band gap, E_g^T, is a parameter. [36, 45] The best-fit values of E_g^T, shown in Fig. 2, also reach their maximum of ~ 2.0 eV at KE_{icp} ~ 90 eV. Similarly, SE measurements reveal a minimum of the extinction coefficient, k(λ = 600 nm), of ta-C films near KE_{icp} = 90 eV. [34] Thus, the optical energy gap is maximized, while optical absorption at a wavelength of 600 nm (near the gap energy) simultaneously is minimized, in ta-C films deposited at KE_{icp} ~ 90 eV. This combination of independent optical and EELS data provides strong evidence that 90 eV is the optimum energy for pulsed-laser deposition of highly diamond-like ta-C films.

Film Uniformity: Spatial Variation of the Optical Band Gap and Film Properties. Measurements of the angular distribution of the C^+ KE_{icp} also were carried out since this determines the maximum area within which spatially uniform film properties can be obtained at any given target-substrate separation, D_{ts}. As shown in Fig. 3, KE_{icp} was nearly constant (±10%) within a half-angular range of 12 to 15 degrees on either side of the plume centerline. At D_{ts} = 10 cm, this corresponds to a 4 to 5 cm long (~ 20 cm^2) region of uniform film properties. It also is interesting to note that SE measurements of ta-C films deposited on 7.5 cm diameter Si wafers, as a function of distance away from the plume center, revealed that the manner in which film properties vary depends on whether the KE_{icp} at the center of the plume is near the 90 eV optimum value or much higher. For example, if KE_{icp} at the plume center is chosen to be only slightly higher than the optimum value then, as shown in Fig. 4, uniform diamond-like properties (E_g^T ~ constant) result over a large central area with properties changing rapidly only further away. However, if a much higher-than-optimum central KE_{icp} ~ 200 eV is used then as shown in Fig. 5 a *degraded* central area is produced (with E_g^T *increasing* away from center) surrounded by a ring of the most diamond-like ta-C, with a rapid fall-off in properties still further away. These different angular dependences of film properties demonstrate again the existence of an optimum KE_{icp} for ta-C film deposition.

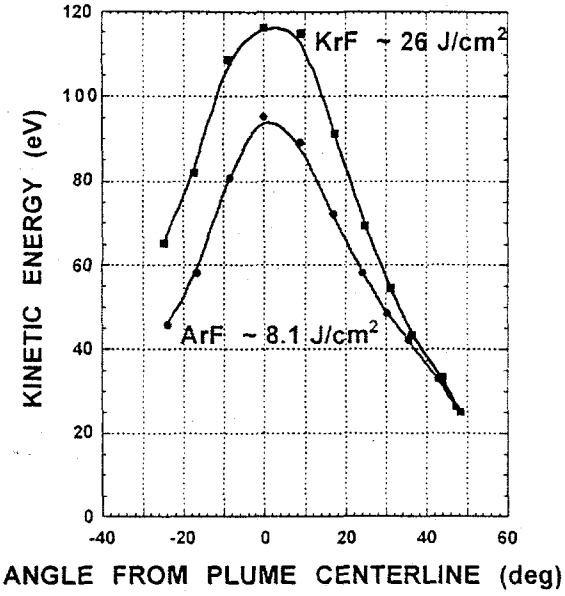

Fig. 3. Angular variation of C^+ ion kinetic energy for ArF (193 nm) and KrF (248 nm) laser ablation of pyrolytic graphite.

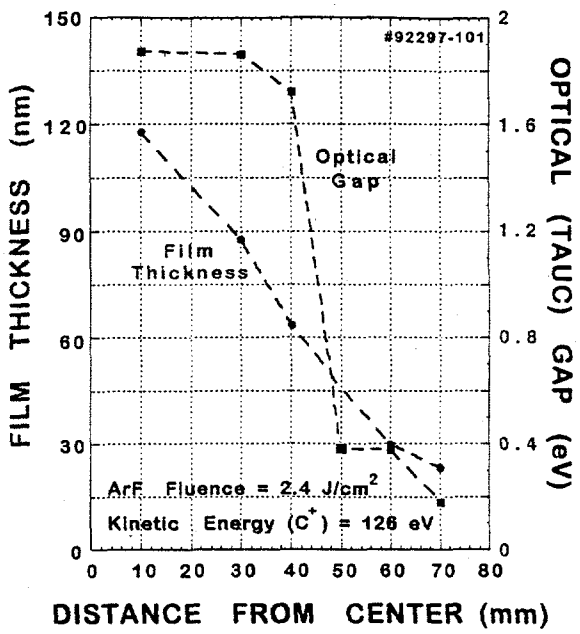

Fig. 4. Spatial variation of film thickness and optical (Tauc) energy gap in a ta-C film deposited at a near-optimum plume-center KE_{icp} of 126 eV.

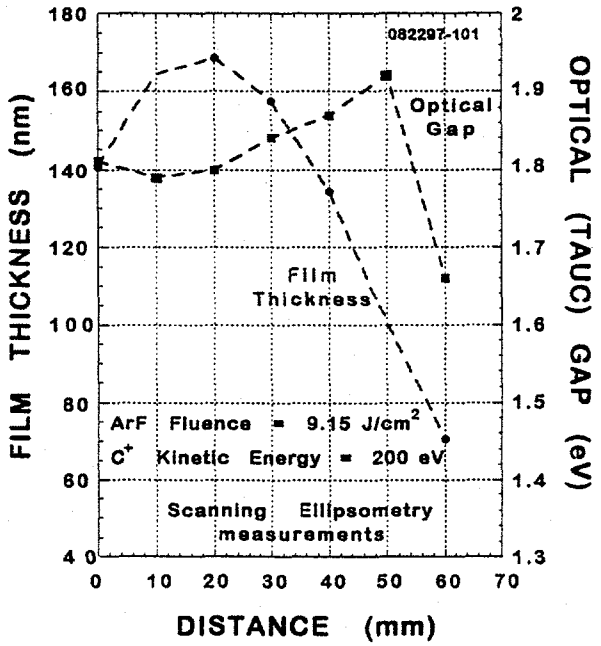

Fig. 5. Spatial variation of film thickness and optical (Tauc) energy gap in a ta-C film deposited at a higher-than-optimum plume-center KE_{icp} of 200 eV.

It is not possible to determine from EELS measurements if the sp^2-bonded carbon in ta-C is uniformly or nonuniformly distributed throughout the film thickness. However, the agreement between the optimum KE_{icp} values determined by EELS (using films only ~ 30 nm thick) and by SE (using 70–180 nm films and assuming a model of a uniform, single-layer film plus two "surface roughness" layers) is at least consistent with a uniform distribution of sp^2 bonds. On the other hand, Siegal et al. quite recently used high-resolution TEM to determine that PLD ta-C films

deposited on silicon actually consist of at least three layers [38]. Two *very thin* low-density layers were found, at the ta-C film's top surface and at the interface with silicon, surrounding a high-density layer that comprised the bulk of the film. The densities and thicknesses of the layers were shown to correlate well with the energetics of the depositing carbon ions [38]. It is not clear whether the model-dependent analysis of SE measurements can meaningfully distinguish between two very thin, low-density surface and interfacial carbon layers on the one hand, and the surface roughness layers that generally are included in SE modeling in order to extract accurate optical constants and layer thicknesses [36]. Thus, there appears to be good overall agreement between the EELS and SE results presented here and the HR-TEM result of Siegal et al. within the limits of the measurements and analysis.

Atomic Force Microscopy: Surface Structure vs Carbon Ion Kinetic Energy. The AFM images shown in Figure 6 reveal that ta-C films deposited at KE_{icp} values of 26, 44, and 90 eV all are quite smooth but still display systematic differences in roughness that are correlated with the KE_{icp} of the C ions used for deposition. The film deposited at 90 eV is extremely smooth with an rms roughness of ~0.9 Å measured over $(200\ nm)^2$ areas. For 26 and 44 eV the corresponding rms roughness values are ~1.6 Å. Similarly, the Z-range of height variation within the $(200\ nm)^2$ area increases from ~0.9 Å (at 90 eV) to ~1.6 Å (at 26 eV). Linear surface-height profiles give very similar results. We note that these energetically deposited carbon films also are relatively free of the large (~ μm scale) particulates sometimes produced by pulsed laser deposition, with typical and largest particulate diameters of ~ 2–10 nm and ~ 100 nm, respectively.

The TM-AFM results of Fig. 6 are in good agreement with the AFM measurements reported by Lifshitz for ta-C films deposited on silicon substrates by the MSIBD method [17]. Lifshitz found a pronounced increase in roughness for films deposited at a carbon ion kinetic energy of 10 eV but very smooth films for kinetic energies ranging from 50 eV up to 10 keV [17]. The broad MSIBD energy range for extremely smooth films overlaps the narrower energy range, from ~30 eV to more than 600 eV, for which MSIBD also produces a high (~80%) sp^3-bonding fraction. [17] The surface roughening found at low energies in both our PLA films and the MSIBD films apparently results from the inability of low-energy C ions to penetrate beneath the surface and form sp^3 bonds, and their subsequent trapping on the surface in a basically graphitic (sp^2-bonded) state. [17] Thus, the surface roughness measurements shown in Fig. 6 and the measurements of sp^3 bonding fraction and film density in Fig. 2 provide a consistent picture of the systematically varying structure and properties of PLA hydrogen-free amorphous carbon films, as a function of the KE used for deposition.

We note that Mercer et al. also used TM-AFM to study the surface morphology of PLA ta-C films deposited using three different KrF (248 nm) laser energy densities, but they first oxygen plasma-etched the films to remove a surface "graphitic carbon" layer. [37] Nanoscale clusters with different sizes and shapes were observed, but the surface roughness of their (plasma-etched) films actually decreased at the lowest laser energy density, contrary to both the results presented here and those of Lifshitz.

In closing this section we note that still more drastic changes in the morphology, bonding and density of PLD carbon films can be produced by ablating a graphite target into an inert-gas ambient and using the gas-phase collisions both to reduce the KE of the carbon ions and to simultaneously induce gas-phase clustering. These effects dramatically change the composition and morphology of PLD carbon films, producing nearly entirely graphitic bonding in "sooty" films that consist of clusters, assemblies of clusters, and "web-like" structures. [39, 40]

Summary: Pulsed-Laser Ablated Amorphous Carbon Films

The combination of ArF laser ablation with in situ ion probe measurements permits ta-C films to be deposited and their properties studied with the mass of the incident species and their kinetic energy reasonably well defined and controlled. This combination was used to make the first (to our knowledge) systematic study of changes in the bonding, optical properties, and surface morphology of pulsed-laser deposited ta-C films as a function of the kinetic energy of the incident species. Striking changes in ta-C film properties were found. EELS measurements reveal that both the sp^3-bonded carbon fraction and the plasmon peak energy (~ electron density) are maximized in films deposited at a C^+ ion energy of ~ 90 eV. Scanning ellipsometry

measurements show that the optical (Tauc) energy gap also is maximized (~ 2.0 eV), resulting in the near-gap optical absorption being minimized, for ta-C film deposition at 90 eV.

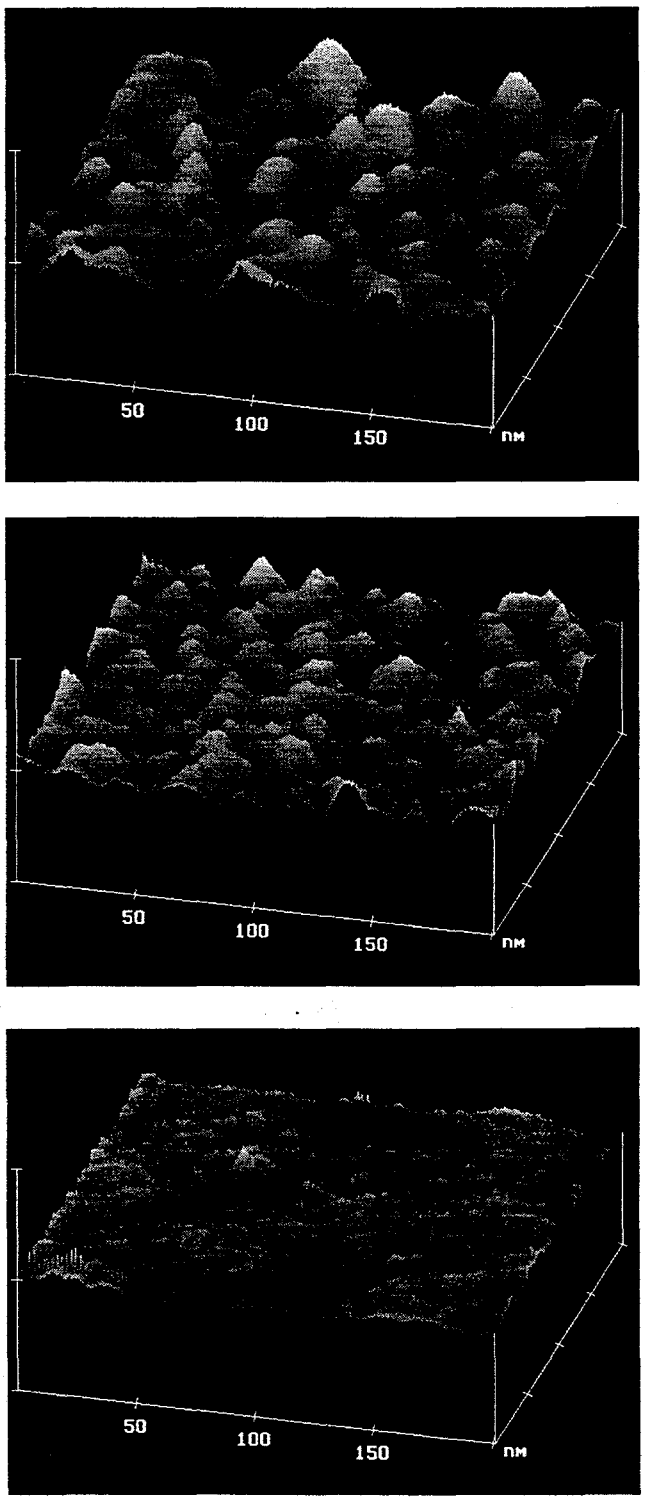

Fig. 6. $(200\ nm)^2$ TM-AFM images of the surfaces of amorphous carbon films deposited at kinetic energies (KE_{icp}) of (top) 26 eV, (middle) 44 eV, and (bottom) 90 eV. [z range = 2 nm]

Measurements of the angular distribution of C^+ kinetic energy show that films with highly uniform (±10%) diamond-like properties are obtained within a half-angular range of at least 12–15 degrees on either side of the plume centerline, corresponding to areas ~ 20 cm^2 at D_{ts} = 10 cm. Finally, tapping-mode atomic force microscope measurements show that films deposited at near-optimum KE are extremely smooth, with rms roughness of only ~ 1 Å over

distances of several hundred nm, and are relatively free of particulates. A small but distinct increase of surface roughness is observed with decreasing C^+ ion KE and is correlated with the increase in sp^2-bonding fraction. In contrast, ablation into an inert-gas background produces "sooty" carbon films with a highly graphitic (sp^2-bonded) structure.

2. Growth of Silicon Microcolumn Arrays

Background

Changes in surface topography resulting in the development of periodic surface structures [48, 49] have been observed in metals, ceramics, polymers and semiconductors as a result of repetitive pulsed-laser irradiation at relatively low laser energy densities, E_d, of less than 1 J/cm^2 [50]. At the higher E_d values (~1-5 J/cm^2) used for pulsed-laser deposition (PLD) of thin films, conical structures are formed in laser ablation targets with the cones aligned along the incident laser-beam direction. [50, 51] The role of the laser wavelength, in controlling the spatial period of near-surface ripple structures, and the efficacy of either a short pulse duration (picosecond or femtosecond) or a short (deep-UV) laser wavelength for precise and efficient material removal (drilling holes or cutting trenches) are among the important results of previous studies. [52, 29] The conical structures produced by sequential laser irradiation have shapes that vary from circular cones to more irregular forms including columns and cone clusters. Most of the models used to explain the development of conical structures assume that they are formed by preferential removal of the material surrounding the cones. The presence of impurities resistant to ablation [53], or surface modification of polymers to produce an ablation-resistant carbon layer [54], or surface segregation conducive to a transparent coating [55], all are models proposed to explain cone formation.

We recently reported new experiments in which arrays of tall, slender silicon microcolumns were formed by cumulative nanosecond pulsed-excimer laser irradiation of a silicon wafer [56]. For example, 1000 pulses of KrF (248 nm) radiation produces ~20-μm tall Si columns with both the average column diameter and their mean separation being ~ 2 μm, as shown in Figure 7. These experiments revealed a succession of topological changes as the number of laser pulses was increased and, through these, it was possible to identify the main features of the mechanism by which high aspect ratio silicon microcolumns are grown. Explaining the formation of microcolumns by cumulative pulsed excimer laser irradiation clearly requires a redeposition (not simply erosion) model and also involves elements of "self-organization". It is proposed that this is an example of "catalyst-free" VLS (vapor-liquid-solid) growth occuring in the ablated flux of Si vapor produced by each laser pulse [56]. The resulting "forests" of high-aspect-ratio columns may be useful as light-trapping anti-reflection coatings or as tips for geometrically enhanced field (cold) emission (FE) of electrons.

Experimental

The experimental procedures have been described elsewhere [56]. Briefly, silicon microcolumns and cones were grown by sequential pulsed KrF (248 nm, 25 ns FWHM pulse duration) excimer laser irradiation of Si wafers, with the number of laser pulses ranging from 200 to 2000. The laser beam was focused with a lens; the irradiated area varied with E_d but was typically 7 mm × 2 mm.

Results

Microcolumns Structure and Morphology. Figure 7 illustrates the ~20 μm-long and ~2-3 μm diameter silicon microcolumns that are formed in air after 1000 laser shots with E_d between 2.7 J/cm^2 and 3.3 J/cm^2. Measurements using a Dektak II profilometer reveal that most of the microcolumns in the center of the laser-irradiated region *protrude above* the original Si surface; typically by 10–15 μm. Microcolumns were formed using commercial n- and p- doped Si wafers of both (001) and (111) orientations. X-ray diffraction measurements show that the crystallographic orientation of the columns is the same as that of the single-crystal Si substrate. No dependence on the magnitude or type of doping was found [56].

Compositional Analysis. Energy dispersive spectroscopy (EDS) analyses performed with conventional and high resolution scanning electron microscopy (SEM) show that the bodies of the microcolumns as well as their tips are mainly silicon. A small amount of oxygen also was detected. Auger emission spectroscopy measurements established that both SiO_2 and Si are present very near the surface of the columns. Auger depth profiling revealed a continuous decrease of oxygen content and a pronounced increase in silicon content with sputtering time, on both the side walls and the tops of the columns [56].

Effect of Ambient Gases. Silicon microcolumn formation was strongly affected by the ambient atmosphere and a series of experiments was carried out in air, N_2, N_2/5% O_2, O_2, SF_6, Ar and Ar/4% H_2, all at atmospheric pressure. These revealed that column formation takes place in an oxygen- or halogen-containing (e.g. fluorine) atmosphere [56]. No columns were formed in the 2.7-3.3 J/cm^2 E_d-range when the atmosphere was N_2, Ar or Ar/4% H_2. Furthermore, it was discovered that the oxygen content of the atmosphere has a large influence on the resulting microcolumn morphology. Smooth, straight columns were obtained when KrF laser irradiation was performed in a N_2-5% O_2 gaseous mixture, whereas in pure oxygen the columns were "plastered" with globules, as though small droplets had been deposited onto the columns' vertical surfaces as well as on their tips [56]. These deposits sometimes formed "canopies" that joined adjacent columns.

The importance of the gas environment was demonstrated also when a plasma etchant, SF_6, was used during column growth. Extremely long structures are produced consisting of cones (that apparently lead the growth) joined by lower walls, which together surround deep central holes, as shown in Figure 8 [56]. The cones protrude more than 20 μm above the original surface. A common feature of the conical structures grown in SF_6 (Fig. 8) and the slender columns grown in an oxygen-containing ambient (Fig. 7) is that both have *droplet-shaped tips*. However, the conical arrays formed in SF_6 are more complex since they show melted droplet-shaped features not only at the tops of the cones and walls but also on their sides (Fig. 8). Another difference is that the cone/wall structures grow in SF_6 at a KrF E_d ~0.9 J/cm^2, which is much lower than the ~3 J/cm^2 E_d-value required to grow columns in an oxygen-containing ambient. We note that Her et al. recently reported that similar conical spikes with spherical caps were produced in 500 Torr of SF_6 or Cl_2 by irradiating silicon wafers with 500 pulses from a 100-fs duration Ti:sapphire (800 nm) laser [57]. The E_d-value in the ~200 μm-diameter center of their Gaussian laser beam also was ~1 J/cm^2. However, the cause of the spherical spikes, including the spherical caps, was considered unknown in their experiments [57].

Systematic Studies of Microcolumn Formation. SEM images provide clues to the nature of the initial column formation and subsequent growth mechanisms:

(1) Redeposition of silicon occurs near the edges and just outside of the laser-ablated region. The redeposited material is easily seen as high elevations in surface-height profiles [56]. Redeposition may come from several sources including small droplets expelled from a transiently laser-melted layer as well as atoms and small clusters that condense back onto the surface.

(2) The smooth and almost vertical column walls, as well as their uniform growth with increasing numbers of laser pulses, suggest that growth occurs by condensation of small atom clusters and/or by molecular reactions at the tips of individual columns. The fact that oxygen and not argon promotes column growth indicates that chemical reactions are involved at the growing tip.

(3) Common to all the columns without exception is the existence of once-molten droplets at their tips. As shown in Fig. 7, these frozen droplets are ~2 μm in diameter.

In order to determine how column growth is initiated, changes in the Si surface morphology were studied in samples irradiated in air with different numbers of laser shots. The main experimental observations are:

(4) After 20 to 50 pulses at 2.7 J/cm^2, fractures develop on the irradiated surface. For (001)-oriented wafers two sets of fracture lines intersecting at 90° form a grid that divides the surface into rectangular blocks with sides 10 μm to 40 μm long. These fractures open up with increasing number of pulses, and deep grooves and very deep craters develop at the fracture walls. The microcolumns then start forming close to the deep grooves. For KrF

irradiation of Si in SF_6 at 0.9 J/cm^2, very deep pits also are formed before conical structures appear on an originally flat Si surface.

(5) A certain number of pulses is required to initiate microcolumn growth. For instance, after 400 KrF pulses at 2.7 J/cm^2 in air only a few columns have formed.

(6) The nucleation of columns is inhomogeneous, taking place always at the sides of deep grooves or pits. New columns nucleate continuously as the number of pulses increases. Correspondingly, when irradiation is stopped after an intermediate number of pulses microcolumns with a range of heights can be observed (Fig. 7).

(7) Silicon microcolumns initially grow rapidly as the number of laser pulses incrreases but growth appears to halt when they reach a certain length. For example, after 600 pulses in air at 2.7 J/cm^2 some of the columns have reached ~40 μm in height. Growth does not continue beyond this limit on additional laser pulses, but nucleation of new columns takes place continuously until a dense "forest" of Si microcolumns has formed.

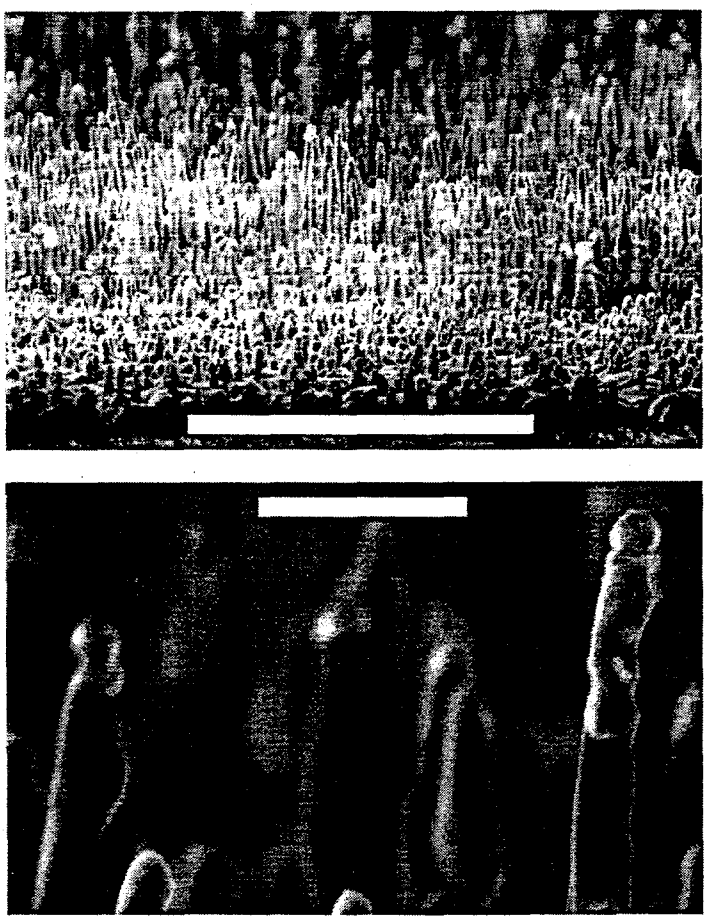

Fig. 7. (Top) SEM image of Si microcolumns formed after 1000 laser shots in air at E_d = 3 J/cm^2 (scale bar = 100 μm). (Bottom) Droplet formed at the tip of a silicon microcolumn (scale bar = 10 μm).

Discussion

Pulsed-Laser Melting of the Tips of Microcolumns. Model calculations show that a KrF laser E_d ~3 J/cm^2 melts a flat Si surface to a depth ~1 μm [58]. The difference between the ~2 μm observed droplet size and the calculated melt depth can be attributed to a lower reflectivity, and correspondingly greater absorption, of the KrF radiation by the Si microcolumns. The model calculations assumed a reflectivity value appropriate for a virgin (flat) Si surface while the experimental reflectivity is expected to be considerably lower due to both cumulative surface roughening and to a thin surface oxide layer that acts as a partial anti-reflection coating [59].

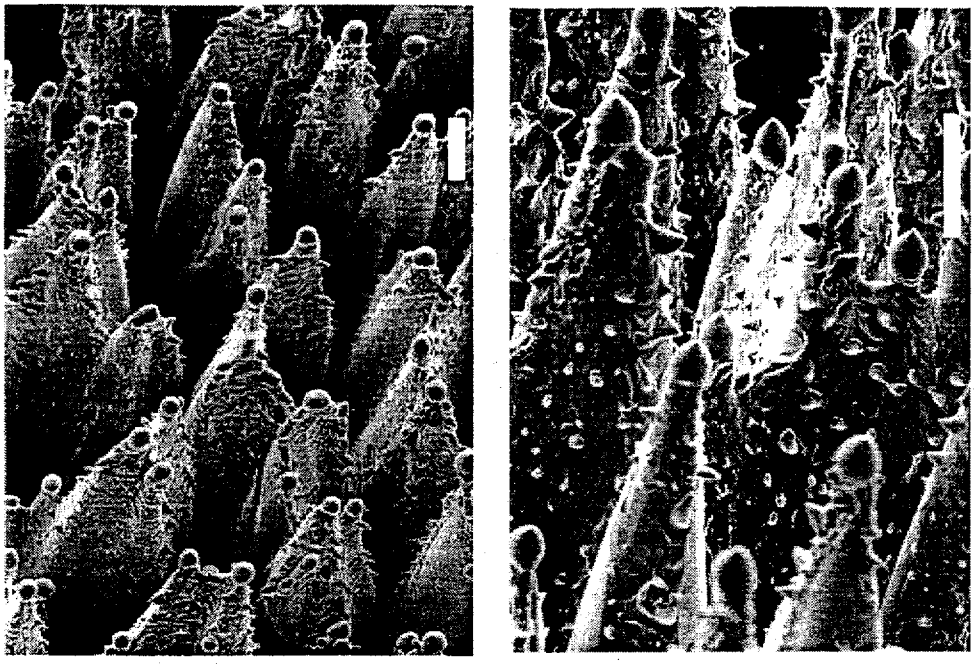

Fig. 8. (Left) Walled Si structure produced by 2040 laser pulses at E_d = 1.5 J/cm^2 in 1 atmosphere of SF_6 (scale bar = 10 μm). (Right) Higher magnification view showing the more complex droplet-like features on the tips of the cones and their side walls (scale bar = 10 μm).

Microcolumn Growth Mechanism. The growth mechanism for silicon microcolumns clearly is different from one involving erosion-resistant column tips because the columns grow above the original surface. The cumulative thermal expansion model described by Kelly and Rothenberg [60] is not applicable because the microcolumn formation and growth observed here is strongly dependent on the ambient atmosphere. In addition, their model would not yield any significant column growth for silicon because thermal expansion in the liquid is mostly compensated by the negative volume change produced upon melting [61].

Based on the results presented above we postulate that the Si microcolumns, once formed, grow as material is deposited on their molten tips. Earlier studies of silicon whisker growth by the VLS method [62, 63] also shed some light on the mechanism of pulsed excimer laser growth of silicon microcolumns and conical structures. In conventional VLS growth, Au clusters are distributed on a Si surface that is heated to a temperature significantly above the Au-Si eutectic at 363°C. The Au clusters alloy with the silicon forming a compound that has a melting point lower than the ambient temperature. When a silicon-rich vapor ($SiCl_4$, SiH_4) is passed over the molten islands, Si dissolves into the melt at its upper surface and precipitates out of solution at the bottom. The result is that a Si whisker grows with the (molten) Au-Si compound remaining at its tip.

In the laser-driven microcolumn growth reported here, each laser pulse re-melts the tip of the column. The sides of the columns do not melt owing to the low laser E_d incident upon them. Each laser pulse also produces melting and an intense flux of silicon-rich vapor from the surface regions between microcolumns. As in conventional VLS growth, the molten tip on top of a solid column acts as a preferred site for silicon deposition. The kinetics of deposition at the droplets is strongly accelerated because the liquid has a high accommodation coefficient [64] and efficiently catalyzes the reaction [63]. If we assume that a silicon droplet remains molten for 200 ns [58] and that a microcolumn grows 20 μm in 200 laser pulses, then the microcolumn growth rate is 100 nm / 200 ns or 0.5 m/s. This high growth rate is the same order of magnitude as the crystal regrowth velocity during pulsed laser annealing of ion implanted silicon [58]. The silicon source for microcolumn growth is the laser-ablated silicon-rich vapor. The role of oxygen (and SF_6) can be seen as silicon etchants that help to produce silicon-containing molecules that can easily attach to the molten droplet at the tip of a microcolumn (or cone). Both the liquid droplet at the tip of a column and the clusters and/or molecules that feed growth at the column tip are produced *essentially simultaneously* by pulsed-laser irradiation, resulting in a new type of *catalyst-free* VLS

growth. However, understanding the precise chemical reaction mechanisms of etching and deposition in the presence of oxygen or halogens requires further experiments and modeling.

Summary: Pulsed-Excimer Growth of Silicon Microcolumns

Dense arrays of silicon microcolumns ~20 to 40 μm tall and ~2 μm in diameter are formed by cumulative nanosecond pulsed excimer laser irradiation of silicon in air and other oxygen-containing atmospheres. Experiments have been carried out that provide insight into the microcolumns initial formation and subsequent growth mechanisms. The microcolumns protrude well above the initial silicon surface and their growth is strongly affected by the gas environment, being enhanced in air or other oxygen-containing ambient. It is proposed that microcolumn growth occurs through a combination of pulsed-laser melting of the tips of the columns and redeposition of silicon from the intense flux of silicon-rich vapor produced by ablation of the surface regions between columns. The molten tips of the columns are strongly preferred sites for deposition, resulting in a high axial growth rate (estimated at ~0.5 m/s) due to the simultaneous production by the pulsed laser of a molten tip and an intense flux of ablated silicon. The process is conceptually similar to the VLS method for silicon whisker growth. However, in pulsed-laser growth of microcolumns no impurity is present to form a eutectic. Instead, the pulsed laser radiation plays two roles almost simultaneously, viz., providing the flux of silicon-containing molecules and melting the tips of the columns.

Acknowledgments

The authors thank S. J. Pennycook for making available the STEM with which the EELS measurements were carried out and P. H. Fleming for assistance with sample preparation. This research was partially sponsored by the Defense Advanced Research Projects Agency under contract DARPA-MIPR-97-1357 with Oak Ridge National Laboratory (ORNL), and by the Office of Basic Energy Sciences, Division of Materials Sciences, U. S. Department of Energy. The research was carried out at ORNL, managed by Lockheed Martin Energy Research Corp. for the U. S. Department of Energy, under contract DE-AC05-96OR22464.

References

1. S. Aisenberg and R. Chabot, *J. Appl. Phys.* **42**, 2953 (1971).
2. I. I. Aksenov et al., *Sov. J. Plasma Phys.* **4**, 425 (1978).
3. J. Robertson, *Prog. Solid State Chem.* **21**, 199 (1991).
4. J. Robertson, *Surf. Coat. Technol.* **50**, 185 (1992).
5. D. R. McKenzie et al., *J. Non-Crystalline Solids* **164-166**, 1101 (1993).
6. For a more complete summary of ta-C film deposition see refs. 10, 11, 13 and 14.
7. D. R. McKenzie, D. Muller, and B. A. Pailthorpe, *Phys. Rev. Lett.* **67**, 773 (1991).
8. R. Lossy et al., *Appl. Phys. Lett.* **61**, 171 (1992).
9. P. J. Fallon et al., *Phys. Rev. B* **48**, 4777 (1993).
10. S. Xu et al., *J. Appl. Phys.* **79**, 7234 (1996).
11. S. Xu et al., *Phil Mag. B* **76**, 351 (1997).
12. W. I. Milne et al., *Mat. Res. Soc. Symp. Proc.* **471**, 231 (1997).
13. S. R. P. Silva et al., *Thin Solid Films* **290-291**, 317 (1996).
14. M. Chhowolla et al., *Phys. Rev. B* **52**, 15812 (1995).
15. J. Kulik et al., *Phys. Rev. B* **52**, 15812 (1995).
16. S. Prawer et al., *Diamond Relat. Mater.* **5**, 433 (1996).
17. Y. Lifshitz, *Diamond Relat. Mater.* **5**, 388 (1996).
18. C. L. Marquardt et al., *Mat. Res. Soc. Symp. Proc.* **38**, 325 (1985).

19. D. L. Pappas et al., *J. Appl. Phys.* **71**, 5675 (1992).
20. D. L. Pappas et al., *J. Appl. Phys.* **72**, 3966 (1992).
21. F. Xiong, Y. Y. Wang, V. Leppert, and R. P. H. Chang, *J. Mater. Res.* **8**, 2265 (1993).
22. F. Xiong, Y. Y. Wang, and R. P. H. Chang, *Phys. Rev. B* **48**, 8016 (1993).
23. A. A. Puretzky et al., *Mat. Res. Soc. Symp. Proc.* **388**, 145 (1995).
24. A. A. Puretzky et al., *Appl. Surf. Sci.* **96-98**, 859 (1996).
25. D. B. Geohegan and A. A. Puretzky, *Mat. Res. Soc. Symp. Proc.* **397**, 55 (1996).
26. D. H. Lowndes et al., *Science* **273**, 898 (1996).
27. K. Yamamoto et al., *Jpn. J. Appl. Phys. Lett.* **36**, L1333 (1997).
28. T. Sato et al., *Jpn. J. Appl. Phys. Lett.* **26**, L1487 (1987).
29. H. Koster and K. Mann, *Appl. Surf. Sci.* **109-110**, 428 (1997).
30. P. T. Murray and D. Thebert-Peeler, p. 359 in Second Inter. Conf. on Laser Ablation: Mechanisms and Applications II, Amer. Inst. of Physics, New York, 1993.
31. J. P. Sullivan, T. A. Friedmann, and A. G. Baca, *J. Electron. Materials* **26**, 1021 (1997).
32. T. A. Friedmann et al., *Appl. Phys. Lett.* **71**, 3820 (1997).
33. M. P. Siegal et al., *Mat. Res. Soc. Symp. Proc.* **349**, 507 (1994).
34. D. H. Lowndes et al., p. 325 in Advances in Laser Ablation of Materials (R. K. Singh et al., eds.), Materials Research Society, Pittsburgh, PA, 1998.
35. V. I. Merkulov et al., accepted by *Applied Physics Letters*.
36. G. E. Jellison, Jr. et al., p. 349 in Advances in Laser Ablation of Materials (R. K. Singh et al., eds.), Materials Research Society, Pittsburgh, PA, 1998.
37. T. W. Mercer et al., *Mat. Res. Soc. Symp. Proc.* **358**, 863 (1995).
38. M. P. Siegal et al., *Appl. Phys. Lett.* **73**, 759 (1998).
39. D. B. Geohegan et al., *Trans. Mater. Res. Soc. Jpn.* **17**, 349 (1994).
40. D. H. Lowndes et al., *Appl. Surf. Sci.* **127-129**, 355 (1998).
41. J. Robertson, *Diamond Relat. Mater.* **2**, 984 (1993).
42. J. Robertson, *Phil. Trans. Royal Soc. London, Ser. A* **342**, 277 (1993).
43. However, we note that Yamamoto et al. recently found for ta-C films deposited by KrF PLA, the sp^3 bonding fraction reased from ~ 26% to ~59% as the fluence was raised from 0.2 J/cm^2 to 7.9 J/cm^2. This increase also was correlated with increasing numbers of more energetic C^+ ions in the ablation plume. See ref. 27.
44. D. B. Geohegan, p. 124-127 and p. 147-8 in Pulsed Laser Deposition of Thin Films (ed. by D. B. Chrisey and G. K. Hubler), John Wiley & Sons, New York, 1994.
45. G. E. Jellison, Jr., and F. A. Modine, *Appl. Phys. Lett.* **69**, 373-373 (1996); ibid. **69**, 2137 (1996).
46. S. D. Berger and D. R. McKenzie, *Phil. Mag. Lett.* **57**, 285 (1988).
47. G. E. Jellison, Jr., and F. A. Modine, *Appl. Opt.* **36**, 8184 (1997); ibid. **36**, 8190 (1997).
48. M. Birnbaum, *J. Appl. Phys.* **36**, 3688 (1965).

49. See the series of three papers by J. F. Young, J. E. Sipe, J. S. Preston, and H. M. van Driel, *Phys. Rev. B* **27**, 1141 (1983); *Phys. Rev. B* **27**, 1155 (1983); *Phys. Rev. B* **30**, 2001 (1984).
50. See S. R. Foltyn, p. 89-113 in Pulsed Laser Deposition of Thin Films (D. B. Chrisey and G. K. Hubler, eds.) Wiley-Interscience, New York, 1994.
51. S. R. Foltyn et al., *Appl. Phys. Lett.* **59**, 594 (1991).
52. P. R. Herman et al., p. 86-95 in Excimer Lasers, Optics, and Applications, Proc. SPIE **2992**, SPIE-The Int. Soc. for Opt. Eng., 1997.
53. P.E. Dyer, F.D. Jenkins, and J. Sidhu, *Appl. Phys. Lett.* **49**, 453 (1986).
54. D.J. Kragnovich and J.A. Vazquez, *J. Appl. Phys.* **73**, 3001 (1992).
55. E.I. Givargizov, *J. Crystal Growth* **20**, 217 (1973).
56. A. J. Pedraza, J. D. Fowlkes, and D. H. Lowndes, submitted to *Applied Physics Letters.*
57. T-H. Her et al., *Appl. Phys. Lett.*. **73**, 1673 (1998).
58. R. F. Wood and G.E. Jellison, Jr., p. 165 in Semiconductors and Semimetals Vol. 23 (R.F. Wood, C.W. White and R.T. Young, eds.) Academic Press, Orlando, FL, 1984.
59. The index of refraction of SiO_2 at 248 nm is n(248) = 1.508 so the SiO_2 thickness required to form a maximally KrF-absorbing coating on silicon is only ~41 nm.
60. R. Kelly and J.E. Rothenberg, *Nucl. Instr. and Methods in Phys. Res. B* **7/8**, 755 (1985).
61. R. Kelly and A. Miotello, p. 55-87 in Pulsed Laser Deposition of Thin Films (D. B. Chrisey and G. K. Hubler, eds.) Wiley-Interscience, New York, 1994.
62. R.S. Wagner, p. 47 in Whisker Technology (A.P. Levitt, ed.) Wiley, New York, 1970.
63. E.I. Givargizov, *Current Topics in Materials Science* **1**, 79 (1978).
64. J.P Hirth and J.M. Pound, *Progr. Mater. Sci.* **11**, 107 (1963).